Organized assembling of poly(ethylene glycol)-functionalized Janus

nanoparticles induced by select alkali metal ions

Jia En Lu and Shaowei Chen*

Department of Chemistry and Biochemistry, University of California, 1156 High Street, Santa

Cruz, California 95064, USA. * E-mail: shaowei@ucsc.edu

Abstract

Gold Janus nanoparticles were prepared by interfacial ligand exchange, with hydrophilic

poly(ethylene glycol) (PEG) ligands on one hemisphere and hydrophobic hexanethiolates on the

other. Due to specific interaction of PEG with alkali metal ions, the Janus nanoparticles exhibited

marked conformational changes forming organized ensembles in the presence of Na⁺ and K⁺, as

manifested in dynamic light scattering, UV-vis absorption and transmission electron microscopic

measurements, whereas no apparent variation was observed with other alkali metal ions (e.g., Li⁺,

Rb⁺), bulk-exchange nanoparticles where the two types of capping ligands were homogeneously

mixed on the nanoparticle surface, or nanoparticles capped with the PEG ligands alone. The ion

complexation was further probed in NMR measurements. Results from this study indicate that

select doping of alkali metal ions into PEG-functionalized nanoparticles may be used for controlled

assembly of the Janus nanoparticles.

Keywords: Janus nanoparticle, poly(ethylene glycol), alkali metal ion, organized ensemble, self-

assembly

Introduction

1

Poly(ethylene glycol) (PEG) represents a family of functional polymer materials that have found diverse applications ranging from industrial manufacturing to medicine [1]. One unique characteristic of PEG is the specific interaction with alkali metal ions, a behavior analogous to crown ethers that can lead to marked enhancement of the electrical conductivity [2-6]. In a previous study [7], it was shown that in the absence of alkali metal ions, triphenylene derivatives containing two to four units of ethylene oxide formed a stable discotic nematic phase (ND) at room temperature, and underwent a unique phase transition to a stable hexagonal columnar (Colh) phase upon the addition of alkali metal ions (e.g., Li⁺ and Na⁺) through ion-dipole interactions, straightening the randomly coiled and bent PEG chains. Self-assembled monolayers of PEG grown on metal substrate surfaces can also be affected by the addition of alkali metal ions [8, 9]. In the absence of alkali metal ions, PEG first self-assembles into small branched dendrite structures with voids at low concentrations on a gold surface; and as the PEG concentration increases, the PEG grows along the terrace steps of gold, and finally adapts the six-fold symmetry of Au(111) [8]. Upon the addition of alkali metal ions, triblock polymers composed of polycaprolactone and poly(ethylene oxide) form multilayered planar structure, sisal-like structure and spherical aggregates upon the addition of Li⁺, Na⁺ and K⁺, respectively [9]. The aggregation disparity is attributed to the structural difference of complex formation between the polymer chains and alkali metal ions of different radii, thus resulting in different self-ensembled alignment and crystallization [10].

In fact, depending on the size of the alkali metal ion and the degree of polymerization of the PEG chain, the interaction kinetics can vary significantly [11, 12]. In contrast to early proposal of the formation of double helical structures [13], recent studies have shown that the interaction of PEG with alkali cations actually leads to the formation of local helical structures, which increases

in length with increasing size of the cation [14]. For instance, cyclic PEG with six repeating units has been found to chelate alkali metal ions of Rb⁺, K⁺, Na⁺, and Li⁺ at 1:1 ratio per nano-cavity (with the highest selectivity towards K⁺), but 2:1 for Cs⁺ due to its larger atomic radius [15]. Linear PEG shows a higher affinity to Li⁺ for chain length shorter than 26 repeat units and higher affinity to Na⁺ for chain length over 26 repeat units [14]. Notably, for cyclic PEG, water-ion bonding interaction is the major contribution to the formation of stable PEG-ion complexes, which becomes increasingly dominant with decreasing size of the alkali metal ion (K⁺ < Na⁺ < Li⁺), and PEG-ion interactions play only a minor role; by contrast, for linear PEG, the primary contribution is the PEG-ion interactions, which increases as the size of the alkali metal ion decreases (K⁺ < Na⁺ < Li⁺), due to the higher cohesion and stability of the PEG-ion complexes when solvated by water [16]. In fact, PEG tends to favor linear conformation for interaction with alkali metal ions in solution, without undergoing significant conformational change [17].

Note that in solution phase, the maximum size/conformation of a polymer can be described by the Flory radius, $F = \alpha n^{3/5}$, where α is the length of each repeating unit and n is the number of repeating units [18]. For PEG-protected nanoparticles in solution, the conformation of PEG on nanoparticle surfaces is in essence dictated by the ratio between the Flory radius (F) and the distance between the attachment points of PEG (D), where PEG exhibits a "mushroom" conformation at low PEG density (D > F) and "brush" conformation at high PEG density (D < F) [19].

Herein, we prepared structurally asymmetrical Janus nanoparticles with hexanethiolates on one face and PEG thiols on the other, and studied the interactions of the nanoparticles with alkali metal ions, in comparison with bulk-exchange nanoparticles where the PEG and hexanethiolate ligands were homogeneously mixed on the nanoparticle surface. The results show that the as-

prepared Janus nanoparticles were individually dispersed in water, whereas upon the addition of Na⁺, formation of organized ensembles occurred due to enhanced rigidity of the PEG ligands and amphiphilicity of the nanoparticle structure, in contrast to the bulk-exchange counterparts.

Experimental Section

Chemicals. Hydrogen tetrachloroaurate trihydrate (HAuCl₄·3H₂O, Fisher, 99%), tetra-noctylammonium bromide (TOABr, Alfa Aesar, 98%), 1-hexanethiol (C6SH, Acros, 96%), sodium
borohydride (NaBH₄, Acros, 99%), and poly(ethylene glycol) methyl ether thiol (PEGSH, SigmaAldrich, average Mn = 800) were used as received. All solvent used were purchased from
commercial sources at their highest purities and used without further treatment. Ultra-pure water
was supplied by a Barnstead Nanopure water system (18.3 M Ω ·cm).

Preparation of hexanethiolate-protected gold (AuC6) nanoparticles. AuC6 nanoparticles were synthesized by using the Brust method [20]. Typically, 30 mL of an aqueous HAuCl₄ solution (0.03 M) was mixed with 20 mL of a toluene solution of TOABr (0.20 M) under vigorous stirring for one hour. The organic phase was then collected, into which was quickly injected 150 μ L of C6SH using an Accumax Pro micropipette. The solution was stirred for 15 min before 24 mL of a freshly prepared, ice-chilled aqueous NaBH₄ solution (0.43 M) was added in a dropwise fashion. The solution showed a dark brown color immediately upon the addition of NaBH₄, indicating the formation of gold nanoparticles. The reaction mixture was stirred for an additional 4 h to reduce the core-size dispersity. The organic phase was then collected and washed five times with methanol to remove excess hexanethiol, phase-transfer catalysts, and reaction byproducts. The average core size of the resulting nanoparticles was determined to be 2.7 \pm 0.4 nm by transmission electron microscopy (TEM) measurements (Figure S1a) [21, 22].

Preparation of PEGSH protected gold (AuPEG) nanoparticles. AuPEG nanoparticles were prepared in a slightly different way. In brief, 30 mL of an aqueous HAuCl₄ solution (0.03 M) was mixed with 20 mL of a toluene solution of TOABr (0.20 M) under vigorous stirring for one hour. The toluene phase was then collected, into which was added 24 mL of a freshly prepared, chilled aqueous NaBH₄ solution (0.43 M) in a dropwise manner. The solution was under magnetic stirring for 8 h before the organic phase was collected and washed at least 3 times with nanopure water. An aqueous PEGSH solution (0.13 g in 15 mL) was then added into the toluene solution. After magnetic stirring for 8 h, the aqueous phase exhibited a dark brown color, signifying successful functionalization of the nanoparticles by the PEGSH ligands. The aqueous phase was collected and washed at least three times with toluene. TEM measurements showed that the average coresize of the resulting AuPEG nanoparticles was 5.6 ± 0.6 nm (Figure S1b).

Preparation of AuC6-PEG Janus nanoparticles. AuC6-PEG JNPs were prepared by interfacial engineering based on the Langmuir method, as detailed previously [21-23]. Briefly, AuC6 nanoparticles obtained above were dispersed in toluene and deposited in a dropwise fashion onto the water surface of a Langmuir-Blodgett trough (NIMA Technology, model 611D) by using a Hamilton microliter syringe. After evaporation of the organic solvent, the nanoparticle monolayer was compressed to a desired surface pressure, where the interparticle spacing was in the intermediate between one and two fully extended C6SH ligand chain lengths, in order to limit particle mobility. A calculated amount of PEGSH was then injected into the water subsurface using a micropipette to allow interfacial ligand exchange reactions to take place. The resulting particles were collected after various reaction times (i.e., 1 h, 2 h, and 6 h) such that a different number of PEGSH ligands were incorporated onto the nanoparticle surfaces. The resulting JNPs (JNP1, JNP2 and JNP6) were purified via centrifugation and re-dispersed in chloroform.

As a control experiment, exchange reactions of the AuC6 nanoparticles with PEGSH were also carried out by mixing a calculated amount of AuC6 nanoparticles and PEGSH ligands in THF and stirred for 48 h. The solution was then dried under reduced pressure with a rotary evaporator and excessive ligands were removed by extensive rinsing with methanol. The resulting particles were denoted as bulk-exchange (BE) particles.

Characterization. The nanoparticle morphologies and sizes were studied using transmission electron microscopy (TEM, Philips CM300 at 300 kV). Contact angle measurements were carried out with a Tantec CAM-PLUS contact angle meter, where nanoparticle monolayers on the Langmuir-Blodgett trough were transferred by down-stroke deposition onto a clean glass slide, except for AuPEG that was deposited by spin-casting. At least ten independent measurements per sample were carried out with a constant water droplet volume of 5 μL for statistical analyses. UV-vis absorption measurements were conducted using a PerkinElmer Lambda 35 UV-vis Spectrometer in a 1 cm quartz cuvette. FTIR spectra were acquired with a PerkinElmer Spectrum One FTIR Spectrometer. Dynamic light scattering (DLS) measurements were carried out with a Wyatt DynaPro NanoStar temperature-controlled micro-sampler. An aliquot (10 μL) of the particle solution (0.015 mg/mL) was introduced into a sample holder via a 20 μL micropipette. Each sample analysis consisted of 50 measurements which were averaged and reported in terms of radius normalized by percent mass. Proton nuclear magnetic resonance (¹H NMR) measurements were performed with a Varian Unity 500 MHz spectrometer.

Results and discussion

AuC6-PEG Janus nanoparticles were prepared by interfacial ligand exchange reaction of AuC6 nanoparticles with PEGSH using the Langmuir-Blodgett method for various reaction times. The resulting nanoparticles (JNP1, JNP2 and JNP6) were collected using down-stroke deposition

method onto cleaned glass slides to allow exposure of the PEG face of the resulting nanoparticles for contact angle measurements. The average contact angle of each sample was shown in Figure 1. The initial AuC6 nanoparticles were highly hydrophobic with an average contact angle of 102.4 \pm 0.8°, whereas the AuPEG nanoparticles were mostly hydrophilic with a much lower average contact angle of 29.2 \pm 1.4°. These are consistent with results obtained previously with alkanethiolate-capped gold nanoparticles and poly(ethylene oxide) [9, 21-24]. For the JNP nanoparticles, the averaged contact angle values were in the intermediate between 50° and 70°, and decreased with increasing reaction time of PEG, JNP1 (64.1 \pm 1.1°) > JNP2 (54.9 \pm 1.0°) > JNP6 (50.7 \pm 0.8°). Note that the BE nanoparticles also exhibited a comparable contact angle of 61.4 \pm 0.8°.

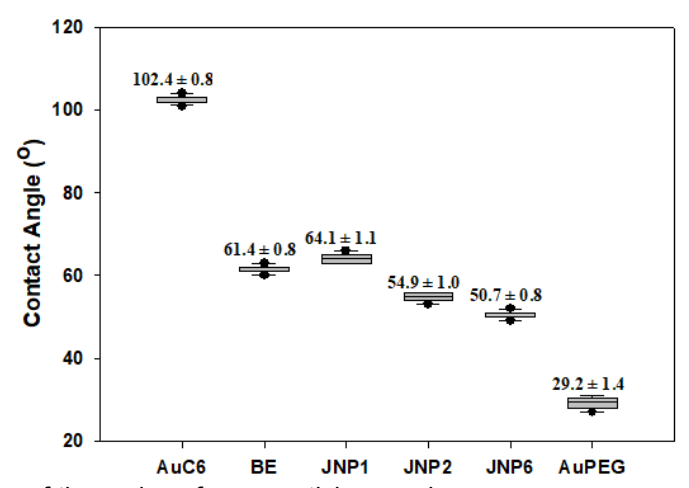


Figure 1. Contact angles of the series of nanoparticle samples.

The incorproation of PEG ligands onto the Janus nanoparticle surface was also confirmed in FTIR measurements (Figure S2a). Specifically, the sp³ C–H vibrational stretches of the C6 ligands can be identified at 2923 cm⁻¹ and that of PEG at 2868 cm⁻¹ [25]. In addition, the C–O stretch of PEG appeared at 1080 cm⁻¹ [26], while the absence of the S–H vibrational stretch at 2550 – 2600 cm⁻¹ indicated that the samples were free of excessive PEGSH ligands. More quantitative analysis of the ligand surface coverage was achieved by ¹H NMR measurements

(Figure S2b). The peak at 0.88 ppm can be ascribed to the methyl protons of the C6 ligands, whereas the peak at 3.28 ppm to the terminal methyl protons of PEG due to deshielding effect from the adjecent oxygen atoms [25]. Based on the integrated peak areas of these methyl protons, the mole fraction of PEG was estimated to be 14.5% for JNP1, 23.7% for JNP2, and 40.8% for JNP6, in comparison to 52.8% for the BE nanoparticles.

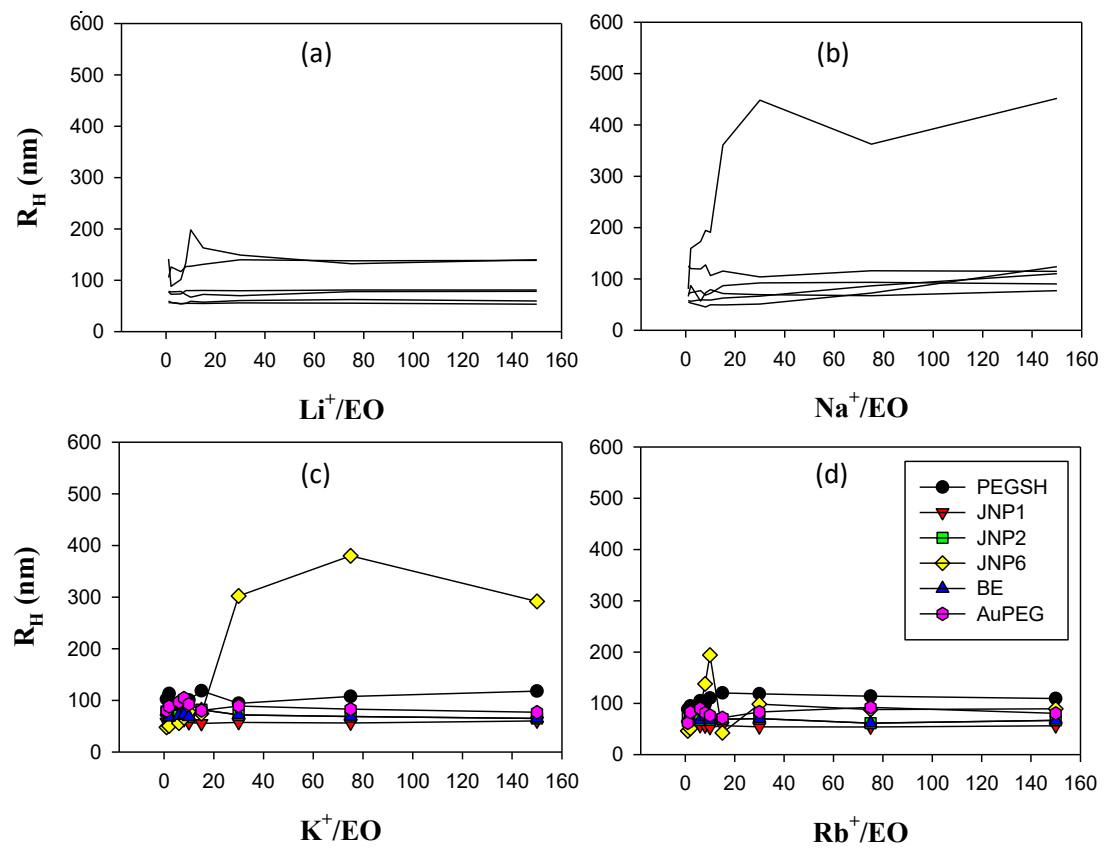


Figure 2. Hydrodynamic radii of PEGSH ligands and nanoparticles (0.015 mg/mL in water) upon the addition of (a) Li⁺, (b) Na⁺, (c) K⁺, and (d) Rb⁺ at different concentrations (expressed as the ratio of alkali metal ions to ethylene oxide units).

Interestingly, upon the addition of alkali metal ions, the nanoparticle structures exhibited a marked variation, as manifested in DLS measurements. Note that based on the Flory radius, the PEG ligands most likely adopted the brush conformation on the Janus nanoparticle surface within the PEG hemisphere, but a mushroom conformation at the PEG/C6 interface [19]. From Figure 2,

it can be seen that the hydrodynamic radius (R_H) of the JNP6 nanoparticles remained virtually unchanged at around 100 nm in the presence of Li⁺ and Rb⁺ even at the metal ion/ethylene oxide (M⁺/EO) ratio of 150, but increased markedly upon the addition of K⁺, for instance, to ca. 300 nm at the K⁺/EO ratio of 30 and remained largely saturated at higher K⁺ concentrations. More drastic enhancement of R_H can be seen with the addition of Na⁺, where R_H was about 400 nm at Na⁺/EO = 30. Note that for the free PEGSH ligands, the R_H was almost unchanged (80-100 nm) even with the addition of these four alkali metal ions at $M^+/EO = 150$, suggesting that the markedly enhanced R_H of JNP6 cannot be accounted for by metal ion-induced conformational transitions of the PEG fragment. Rather, it is likely that the binding of select alkali metal ions led to the formation of organized assembly of the nanoparticles (vide infra). Such a variation of the R_H change can be attributed to the different "cloud point" effect on the PEG chain upon the addition of different alkali metal ions [27-29], which has been found to decrease in the order of K⁺> Rb⁺> Cs⁺> Na⁺ > Li⁺ [29]. The fact that R_H remains invariant upon the addition of Li⁺ suggests that the PEG conformation is mostly insensitive of the PEG-Li interaction [28]; yet upon the addition of Na⁺ and K⁺, the significant R_H variations observed indicate drastic structural change of PEG, where the enhanced rigidity of the PEG segments facilitated the exposure of the hydrophobic C6 ligands and resulted in the self-assembly of JNP6 forming organized ensembles [21-23, 30, 31]. By contrast, due to the large atomic radius of Rb⁺, the ions mostly interacted only with the outer portion of the PEG chain instead of diffusing into the interior, and the resulting conformational change of PEG was not sufficient to lead to self-assembly of JNP6. In fact, one can see that the BE nanoparticles, despite a similar PEG surface coverage to that of JNP6 but with ligands homogeneously mixed on the nanoparticle surface, showed no variation of the R_H even at M⁺/EO up to 150. Furthermore, JNP1, JNP2 and AuPEG showed rather consistent R_H (80-100 nm), and the radii did not change

appreciably with the ion concentration increased to $M^+/EO = 150$. This suggests that (i) the PEG coverage on the nanoparticle surface did not significantly impact the R_H , and (ii) no organized assembly was formed for these nanoparticles, likely because low amphiphilicity of JNP1 and JNP2, and monofunctionalization of AuPEG.

Consistent results were obtained in TEM measurements. From the TEM micrographs in Figure 3, one can see that after the addition of Na⁺ at Na⁺/EO = 30, JNP1 and JNP2 remained well dispersed without apparent agglomeration (panels a and b), similar to that with BE nanoparticles (panel d), whereas formation of nanoparticle ensembles (a few hundred nm across) was apparent with JNP6 nanoparticles (panel c). It should be noted that in the absence of alkali metal cations, JNP6 nanoparticles were well dispersed in water without apparent agglomeration (Figure S3). This is different from the behaviors that we observed earlier with JNPs capped with short hydrophilic ligands (e.g., 3-mercapto-1,2-propanediol), where the nanoparticles were found to self-assemble into organized ensembles even in the absence of metal ions [21, 22, 32]. Such a discrepancy suggests that the AuC6-PEG JNP6 nanoparticles did not exhibit amphiphilic characters in solution, most likely due to the long, flexible PEG chains that extended over the C6 hemisphere and limited the exposure of the hydrophobic C6 ligands.

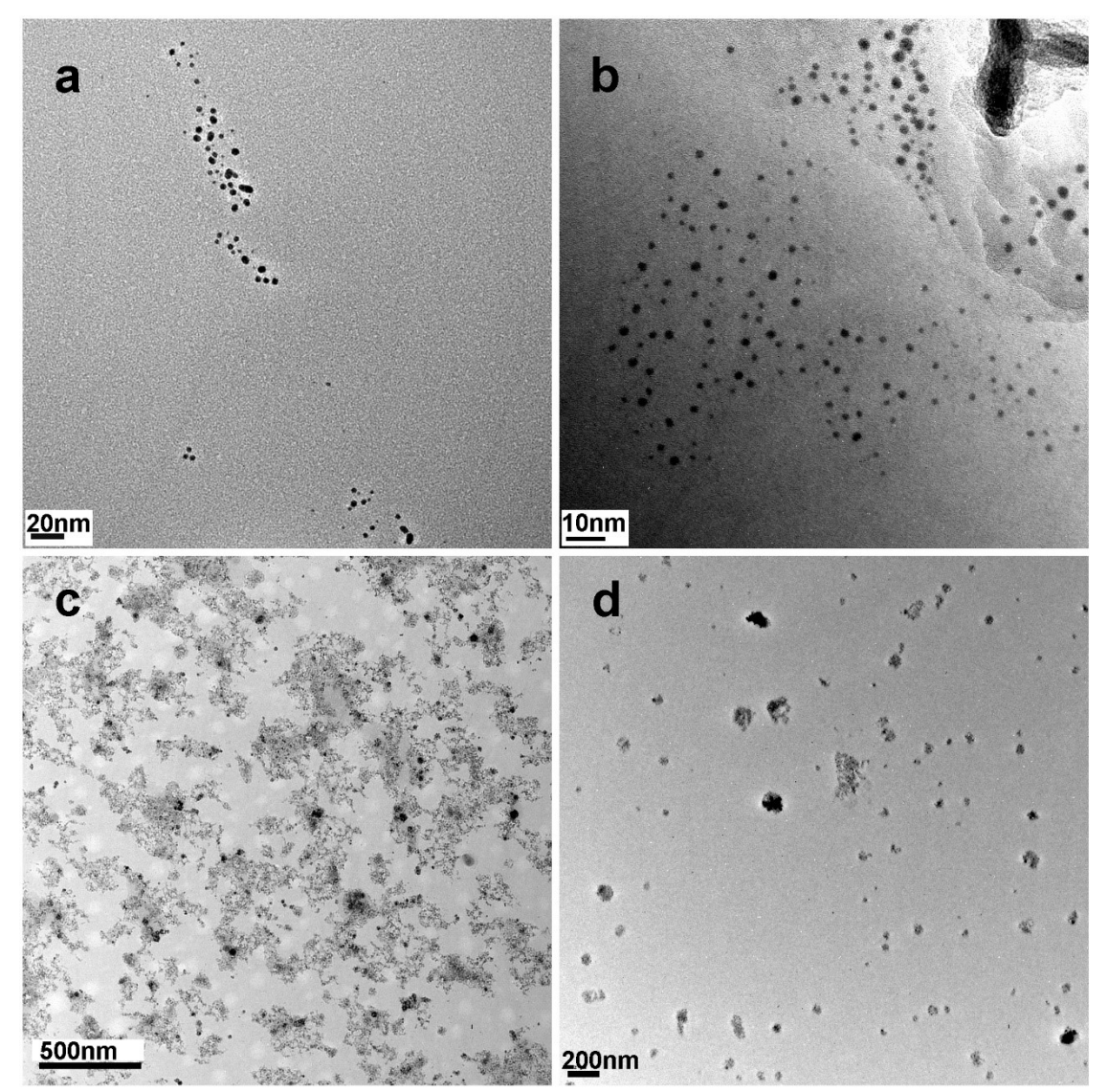


Figure 3. TEM images of (a) JNP1,(b) JNP2, (c) JNP6 and (d) BE upon addition of Na⁺ at the Na⁺/EO ratio of 30. Nanoparticle concentrations all 0.015 mg/mL in water.

Such structural variations are schematically depicted in Figure 4a. Because of the long chain legth of the PEG ligands in comparision to C6, the PEG ligands on as-prepared JNP6 likely adopted a mushroom conformation at the PEG/C6 interface, thus rendering the nanoparticles individually dispersible in water. Upon the addition of select alkali metal ions such as Na⁺, the PEG chains became structurally rigid [7], which led to exposure of the hydrophobic C6 ligands. The resulting amphiphilic characters of the nanoparticles allowed self-assembly of the

nanoparticles into organized ensembles, akin to conventional surfactant molecules [21, 22, 32]. Lesser effects were observed with other metal ions, suggesting insignificant conformational change of the PEG ligands [28]. In fact, results from UV-vis absorption studies (Figure 4b and S3) show that in the absence of alkali metal ions, the JNP6 nanoparticles exhibited a surface plasmon resonance (SPR) at ca. 520 nm, characteristic of well dispersed gold nanoparticles [33]; and upon the addition of Na⁺, the SPR peak can be seen to become broadened and red-shift to 550 nm, two signatory behaviors of the formation of nanoparticle ensembles [32]. In addition, the relatively small SPR shift of JNP6 (from 520 nm to 550 nm) in comparison to that observed in the previous studies with much shorter hydrophilic ligands (> 600nm) [21, 22] is also in agreement with the formation of small nanoparticle ensembles, as seen in the TEM images (Figure 3c). By sharp contrast, no apparent variation was observed for other nanoparticles in the series (i.e., JNP1, JNP2, BE, and AuPEG), suggesting the lack of ensemble formation of these samples, again, in good agreement with the TEM results (Figure 3a, b, and d).

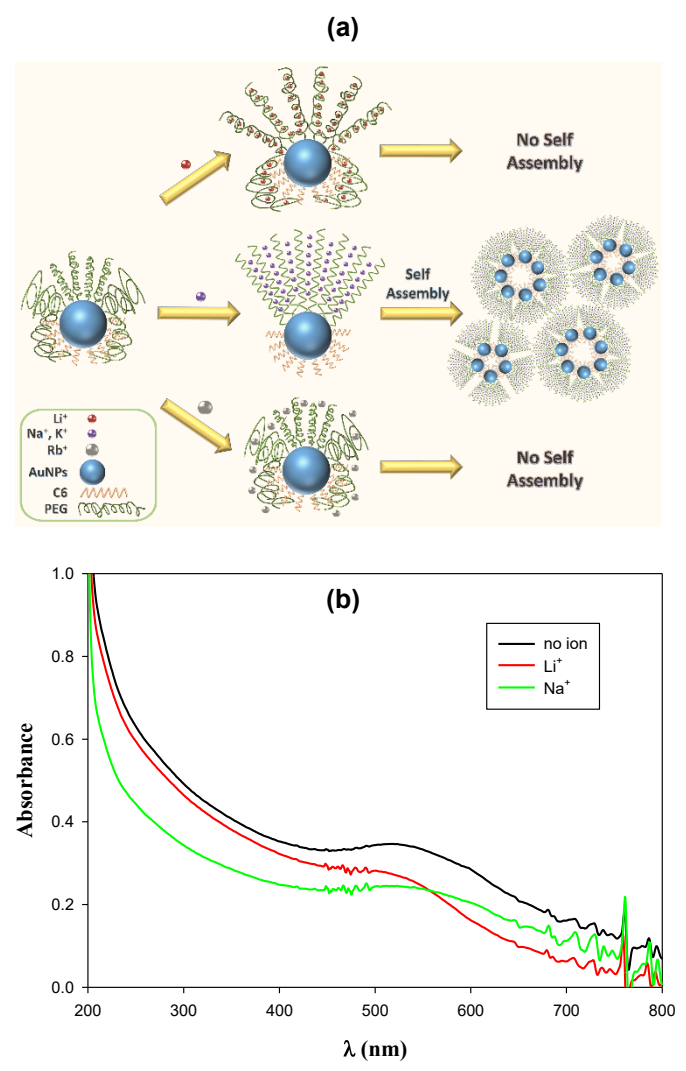


Figure 4. (a) Schematic of alkali metal ions induced self-assembly of PEG-functionalized Janus nanoparticles. (b) UV-vis absorption spectra of JNP6 nanoparticles in the absence and presence of Li⁺ and Na⁺ at the M⁺/EO ratio of 30. Nanoparticle concentration 0.015 mg/mL in water.

The interactions of alkali metal ions with the PEG ligands can also be probed by the change of chemical shift and peak broadening/splitting in ¹H NMR measurements [34-38]. In general, the chemical shift indicates the interaction strength between different species, and in the present study, the interaction between PEG and alkali metal ions [39]. On the other hand, the sharpness of NMR peaks can be correlated to the coupling of neighboring protons, where enhanced dipolar coupling between neighboring protons leads to broadening and even splitting of a peak signal [34]. From

Figure 5a, one can see that prior to the addition of alkali metal ions, the PEGSH monomeric ligands, AuPEG and JNP6 all show a peak at 3.55 ppm, which can be ascribed to the ethylene protons (-CH₂-CH₂-O-) of the PEG chains [40]. The appearance of a sharp singlet is most likely due to the formation of a stable distotic nematic (N_D) phase of the long polymer chains at room temperature [7] and hence chemical equivalence of the ethylene protons due to the fast proton exchance rate [34]. Interestingly, upon the addition of Li⁺ and Na⁺ ions (and gentle mixing for 30 min), the ethylene proton peak was broadened, and split into a semi-doublet, indicating chemical inequivalence of the ethylene protons that most likely arose from the formation of PEG-ion complexes. This may be ascribed to a phase transition of PEG from its stable N_D phase to hexagonal columnar (Colh) phase [7], which lowered the chain mobility by electronic attraction between the cations and PEG [41]. Similar behaviors have been observed in previous studies with crown ethers, where upon coordination with alkali metal ions, the NMR signal of the ethylene protons (3.73 ppm) was found to split into two sets of signals (3.50/3.78 ppm for Na⁺ and 3.68/3.83 ppm for Li⁺) [36]. In the present study, the chemical shift of the ethylene protons of PEGSH can be seen to move downfield to 3.66 ppm and 3.61 ppm upon the addition of Li⁺ and Na⁺, respectively, indicating comparable, apparent interaction between PEG and the tien ions due to the formation of PEG-cation complex, where the deshielding effect lowered the electron density around the ethylene protons of adjacent carbons [39]. The slightly smaller shift for Na⁺ can be correlated to the cloud point effect for the PEG ligands upon the addition of Na⁺, where the PEG-Na⁺ complexation was achieved by two neighboring PEG chains brought together by the cloud point effect, which lessened the deshielding effect of the PEG protons and reduced the downfield shift. By contrast, the cloud point effect on the PEGSH ligands in the presence of Li⁺ is minimal (no PEG aggregation, as shown in Figure 2), so the deshielding effect on PEGSH proton is larger

due to stronger interaction between the oxygen on PEGSH (most likely on the same polymer chain) and Li⁺.

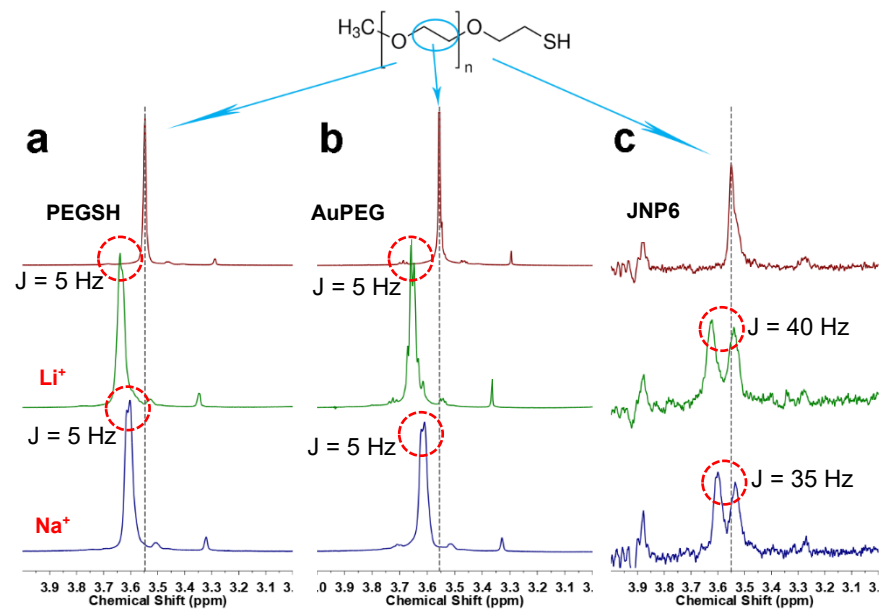


Figure 5. ¹H NMR spectra of (a) PEGSH, (b) AuPEG and (c) JNP6 in the absence (top curves) and presence of Li⁺ (middle curves) and Na⁺ (bottom curves) in CD₃CN at M⁺/EO = 30

Similar behaviors were observed with AuPEG, where the ethylene peaks were shifted to 3.64 ppm and 3.61 ppm upon the addition of Li⁺ and Na⁺ ions, respectively (Figure 5b), indicating similar ion binding behaviors between free PEGSH ligands and those bound onto the AuPEG nanoparticle surface. Nevertheless, one can see that the splitting of the ethylene protons for AuPEG upon the interaction with Li⁺ became better defined with a coupling constant of J = 5 Hz (which is similar to that of free PEGSH ligands). This chemical inequivalence of the ethylene proton demonstrated that the specific binding of Li⁺ ion to the PEG structure brought the ethylene protons closer to each other by slowing the PEG chain mobility and hence led to apparent dipolar coupling between protons attached on the adjacent carbons [40]. By contrast, the peak splitting was slightly less significant with Na⁺, likely due to the larger size of Na⁺ forming larger PEG-cation complex, which results in weaker inter-/intra-molecular coupling between protons. Furthermore, the high

PEG content on AuPEG might also limit the Na⁺ diffusion into the interior of the PEG capping layer, thus the change of chain mobility and chemical environment for ethylene proton were not as high as for the Li⁺-doped sample.

For JNP6, the spiltting was far more prounced (Figure 5c). Specifically, upon the addition of Li⁺ and Na⁺ ions, the ethylene proton peak splits into a broad and well-defined doublet, at 3.54/3.62 ppm and 3.53/3.60 ppm, with a coupling constant of J = 40 Hz and 35 Hz, respectively. This suggests a much enhanced incorporation of alkali metal ions forming stable PEG-cation complexes that highly reduced the PEG chain mobility, thus enhanced the differentiation of the protons on the same methylene carbon, leading to strong dipolar coupling between protons attached on the same carbon (i.e., $H_a-H_{a'}$ and $H_b-H_{b'}$ for $-O-CH_aH_{a'}-CH_bH_{b'}-O-$) [37, 38]. Unlike the coupling between protons attached to adjacent carbons, chemical inequivalence of protons on the same carbon without a chiral center is a strong indication of the formation of an organized coordination structure with one proton interacting with the metal center while the other is not (pointing outwards in a crown-ether-like / helical structure) [34]. This different proton positioning resulted in chemical inequivalence which gave rise to the broadening of the doublet signal. The markedly greater peak broadening and splitting observed with JNP6, in comparison to AuPEG, can be attributed to the ligand segregation on JNP6 that facilitates metal cation incorporation forming stable PEG-cation complexes, which limits the chain mobility and results in more apparent signal change.

Conclusion

In this study, AuC6-PEG Janus nanoparticles with a PEG hemisphere showed unique binding affinity to alkali metal ions. The as-prepared Janus nanoparticles were found to be individually dispersed in water, likely due to the much longer PEG ligands that adopted a mushroom conformation, especially at the PEG/C6 ligand interface. Upon the addition of select alkali metal ions (e.g., Na⁺), the formation of PEG-cation complex led to enhanced rigidity of the PEG ligand chains, and hence exposure of the hydrophobic C6 hemisphere. The resulting amphiphilic characters rendered the nanoparticles to self-assemble into organized ensembles, as manifested in DLS and TEM measurements and further confirmed by NMR measurements. These unique properties may be exploited for select chemical doping of PEG-functionalized nanoparticles, controlled assembly of the nanoparticles, as well as chemical sensing of alkali metal ions.

Acknowledgements

This work was supported, in part, by the National Science Foundation (CHE-1710408 and CBET-1848841). TEM work was performed at the National Center for Electron Microscopy, Lawrence Berkeley National Laboratory, as part of a user project.

Appendix A. Supplementary materials

Supplementary data to this article can be found online at https://doi.org/10.1016/...

References

- [1] J.S. Suk, Q.G. Xu, N. Kim, J. Hanes, L.M. Ensign, PEGylation as a strategy for improving nanoparticle-based drug and gene delivery, Adv Drug Deliver Rev, 99 (2016) 28-51.
- [2] Z.G. Xue, D. He, X.L. Xie, Poly(ethylene oxide)-based electrolytes for lithium-ion batteries, J Mater Chem A, 3 (2015) 19218-19253.
- [3] A.M. Stephan, Review on gel polymer electrolytes for lithium batteries, Eur Polym J, 42 (2006) 21-42.
- [4] C.H. Zhang, S. Gamble, D. Ainsworth, A.M.Z. Slawin, Y.G. Andreev, P.G. Bruce, Alkali metal crystalline polymer electrolytes, Nat Mater, 8 (2009) 580-584.
- [5] H. Li, X.T. Ma, J.L. Shi, Z.K. Yao, B.K. Zhu, L.P. Zhu, Preparation and properties of poly(ethylene oxide) gel filled polypropylene separators and their corresponding gel polymer electrolytes for Li-ion batteries, Electrochim Acta, 56 (2011) 2641-2647.
- [6] D. Saikia, H.Y. Wu, Y.C. Pan, C.P. Lin, K.P. Huang, K.N. Chen, G.T.K. Fey, H.M. Kao, Highly conductive and electrochemically stable plasticized blend polymer electrolytes based on PVdF-HFP and triblock copolymer PPG-PEG-PPG diamine for Li-ion batteries, J Power Sources, 196 (2011) 2826-2834.

- [7] S. Kohmoto, E. Mori, K. Kishikawa, Room-temperature discotic nematic liquid crystals over a wide temperature range: Alkali-metal-ion-induced phase transition from discotic nematic to columnar phases, J Am Chem Soc, 129 (2007) 13364-+.
- [8] J. Rundqvist, J.H. Hoh, D.B. Haviland, Poly(ethylene glycol) self-assembled monolayer island growth, Langmuir, 21 (2005) 2981-2987.
- [9] J.B. Fan, F. Long, Z.W. Liang, M.P. Aldred, M.Q. Zhu, Hierarchical mesostructures of biodegradable triblock copolymers via evaporation-induced self-assembly directed by alkali metal ions, Colloid Polym Sci, 290 (2012) 1637-1646.
- [10] Y. Inokuchi, O.V. Boyarkin, R. Kusaka, T. Haino, T. Ebata, T.R. Rizzo, UV and IR Spectroscopic Studies of Cold Alkali Metal Ion-Crown Ether Complexes in the Gas Phase, J Am Chem Soc, 133 (2011) 12256-12263.
- [11] G.R.C. Hamilton, S.K. Sahoo, S. Kamila, N. Singh, N. Kaur, B.W. Hyland, J.F. Callan, Optical probes for the detection of protons, and alkali and alkaline earth metal cations, Chem Soc Rev, 44 (2015) 4415-4432.
- [12] Z.Z. Cai, L.H. Do, Customizing Polyolefin Morphology by Selective Pairing of Alkali Ions with Nickel Phenoxyimine-Polyethylene Glycol Catalysts, Organometallics, 36 (2017) 4691-4698.
- [13] J.M. Parker, P.V. Wright, C.C. Lee, A Double Helical Model for Some Alkali-Metal Ion-Poly(Ethylene Oxide) Complexes, Polymer, 22 (1981) 1305-1307.
- [14] K. Shimada, S. Matsuyama, T. Saito, S. Kinugasa, R. Nagahata, S. Kawabata, Conformational effects on cationization of poly(ethylene glycol) by alkali metal ions in matrix-assisted laser desorption/ionization time-of-flight mass spectrometry, Int J Mass Spectrom, 247 (2005) 85-92.
- [15] T. Terashima, M. Kawabe, Y. Miyabara, H. Yoda, M. Sawamoto, Polymeric pseudo-crown ether for cation recognition via cation template-assisted cyclopolymerization, Nat Commun, 4 (2013) 2321.
- [16] L. Poudel, R. Podgornik, W.Y. Ching, The Hydration Effect and Selectivity of Alkali Metal Ions on Poly(ethylene glycol) Models in Cyclic and Linear Topology, J Phys Chem A, 121 (2017) 4721-4731.
- [17] L. Chai, R. Goldberg, N. Kampft, J. Klein, Selective adsorption of poly(ethylene oxide) onto a charged surface mediated by alkali metal ions, Langmuir, 24 (2008) 1570-1576.
- [18] P.G. de Gennes, Polymers at an interface; a simplified view, Advances in Colloid and Interface Science, 27 (1987) 189-209.
- [19] J.V. Jokerst, T. Lobovkina, R.N. Zare, S.S. Gambhir, Nanoparticle PEGylation for imaging and therapy, Nanomedicine, 6 (2011) 715-728.
- [20] M. Brust, M. Walker, D. Bethell, D.J. Schiffrin, R. Whyman, Synthesis of Thiol-Derivatized Gold Nanoparticles in a 2-Phase Liquid-Liquid System, J Chem Soc Chem Commun, (1994) 801-802.
- [21] J.E. Lu, C.H. Yang, H.B. Wang, C.Y. Yam, Z.G. Yu, S.W. Chen, Plasmonic circular dichroism of vesicle-like nanostructures by the template-less self-assembly of achiral Janus nanoparticles, Nanoscale, 10 (2018) 14586-14593.
- [22] J.E. Lu, Y. Peng, S.W. Chen, Janus Nanoparticle Emulsions as Chiral Nanoreactors for Enantiomerically Selective Ligand Exchange, Part Part Syst Char, (2019) 1800564.
- [23] S. Pradhan, L.P. Xu, S.W. Chen, Janus nanoparticles by interfacial engineering, Adv Funct Mater, 17 (2007) 2385-2392.
- [24] Y. Song, K. Liu, S.W. Chen, AgAu Bimetallic Janus Nanoparticles and Their Electrocatalytic Activity for Oxygen Reduction in Alkaline Media, Langmuir, 28 (2012) 17143-17152.
- [25] R.M. Silverstein, Spectrometric Identification of Organic Compounds, Seventh ed., John Wiley & Sons, Inc. 2005.
- [26] B.W. Chieng, N.A. Ibrahim, W.M.Z.W. Yunus, M.Z. Hussein, Poly(lactic acid)/Poly(ethylene glycol) Polymer Nanocomposites: Effects of Graphene Nanoplatelets, Polymers, 6 (2014) 93-104.
- [27] E. Florin, R. Kjellander, J.C. Eriksson, Salt effects on the cloud point of the poly(ethylene oxide)+ water system, J Chem Soc, Faraday Trans 1: Phys Chem Cond Phases, 80 (1984) 2889-2910.

- [28] Y. Masuda, T. Nakanishi, Ion-specific swelling behavior of poly(ethylene oxide) gel and the correlation to the intrinsic viscosity of the polymer in salt solutions, Colloid Polym Sci, 280 (2002) 547-553.
- [29] C.-l. Ren, W.-d. Tian, I. Szleifer, Y.-q. Ma, Specific Salt Effects on Poly(ethylene oxide) Electrolyte Solutions, Macromolecules, 44 (2011) 1719-1727.
- [30] Q. Xu, X.W. Kang, R.A. Bogomolni, S.W. Chen, Controlled Assembly of Janus Nanoparticles, Langmuir, 26 (2010) 14923-14928.
- [31] Y. Song, S.W. Chen, Janus Nanoparticles: Preparation, Characterization, and Applications, Chem Asian J, 9 (2014) 418-430.
- [32] Y. Song, S.W. Chen, Janus Nanoparticles as Versatile Phase-Transfer Reagents, Langmuir, 30 (2014) 6389-6397.
- [33] J.A. Creighton, D.G. Eadon, Ultraviolet Visible Absorption-Spectra of the Colloidal Metallic Elements, J Chem Soc-Faraday Trans, 87 (1991) 3881-3891.
- [34] K. Flodstrom, H. Wennerstrom, V. Alfredsson, Mechanism of mesoporous silica formation. A time-resolved NMR and TEM study of silica-block copolymer aggregation, Langmuir, 20 (2004) 680-688.
- [35] I. Tiritiris, T. Schleid, K. Muller, Solid-state NMR studies on ionic closo-dodecaborates, Appl Magn Reson, 32 (2007) 459-481.
- [36] R.C. Brachvogel, H. Maid, M. von Delius, NMR Studies on Li+, Na+ and K+ Complexes of Orthoester Cryptand o-Me-2-1.1.1, Int J Mol Sci, 16 (2015) 20641-20656.
- [37] L.Y. Yang, X.B. Fu, T.Q. Chen, L.K. Pan, P. Ji, Y.F. Yao, Q. Chen, Ionic Conductivity of beta-Cyclodextrin-Polyethylene-Oxide/Alkali-Metal-Salt Complex, Chem-Eur J, 21 (2015) 6346-6349.
- [38] Y.J. Lee, T.H. Ho, C.C. Lai, S.H. Chiu, Size effects in the alkali metal ion-templated formation of oligo(ethylene glycol)-containing [2]catenanes, Org Biomol Chem, 14 (2016) 1153-1160.
- [39] D.M. Wang, Y. Aso, H. Ohara, T. Tanaka, Synthesis and Characterization of Alkali Metal Ion-Binding Copolymers Bearing Dibenzo-24-crown-8 Ether Moieties, Polymers, 10 (2018) 1095.
- [40] R.M. Silverstein, F.X. Webster, D.J. Kiemle, D.L. Bryce, Spectrometric Identification of Organic Compounds, 8th Ed., (2014).
- [41] M. Irandoust, H. Daraei, R. Rostamian, Proton NMR probing of stoichiometry and thermodynamic data for the complexation of Na+ and Li+ ions with 15-Crown-5 in acetonitrile-nitrobenzene mixtures, Polyhedron, 30 (2011) 1207-1212.